Al-Aqar R, Atahan A, Benniston AC, Perks T, Waddell PG, Harriman A.

Exciton Migration and Surface Trapping for a Photonic Crystal Displaying Charge-Recombination Fluorescence.

***Chemistry: A European Journal* (2016)**

DOI: 10.1002/chem.201602155

FULL PAPER

Exciton Migration and Surface Trapping for a Photonic Crystal Displaying Charge-Recombination Fluorescence

Roza Al-Aqar,[a] Alparslan Atahan,[a,b] Andrew C. Benniston,[a] Thomas Perks,[a] Paul G. Waddell[c] and Anthony Harriman*[a]

Dedication: This work is dedicated to Dr. Raymond Ziessel on the occasion of his retirement from the University of Strasbourg.

Abstract: A compact donor-acceptor molecular dyad has been synthesized by attaching an N,N-dimethylamino fragment to a naphthalic anhydride residue. The dyad shows fluorescence from an intramolecular charge-transfer state (i.e., charge-recombination fluorescence) in fluid solution, with the photophysical properties being strongly dependent on the solvent polarity. Similar emission is seen for single crystals of the target compound, molecules being aligned head-to-head, although time-resolved emission profiles display dual-exponential kinetics. A second polymorph having the head-to-tail alignment also gives rise to two lifetimes, these differ somewhat from those of the first structure, which are assigned to bulk and surface-bound molecules. Growing the crystal in the presence of Rhodamine B localizes the dye around the surface. Excitation of the crystal is followed by sub-ps exciton migration along the aligned stacks, with occasional crossing to adjacent stacks and trapping at the surface. Rhodamine B present at very low levels acts as the acceptor for excitons entering the surface layer. Crystals embedded in a polyester resin form an artificial light-harvesting antenna able to sensitize an amorphous silicon solar cell.

Introduction

Natural photosynthetic organisms employ elaborate light-harvesting machinery to collect sunlight over a wide spectral range and channel the absorbed excitons to a specific site where redox chemistry takes place.[1,2] There are several disparate types of light-harvesting arrays,[3] each selected according to the particular demands of the organism, displaying varying levels of sophistication.[4,5] The primary function of these photon concentrators is to supply the catalytic site with a steady flux of excitons of appropriate energy such that multi-electron fuel formation can proceed without exposing the local environment to highly energetic intermediate species. Artificial photosynthetic systems designed[6-8] as bio-inspired analogues have tended to avoid the light-harvesting antennae in favor of focusing on the light driven electron-transfer chemistry.[9,10] The rather limited progress that has been made in the field,[11] despite major advances in the synthesis of intricate molecular assemblies which closely resemble the photosynthetic reaction center complex, might be used to argue that light-harvesting is crucial to the successful storage of sunlight as chemical potential.[12]

Light-harvesting antennae operate by arranging selected fluorophores in close proximity such that efficient electronic energy transfer (EET) can occur between neighboring chromophores. Many artificial molecular arrays have been described that duplicate such EET processes.[13-16] In a few cases, EET occurs over a dozen or so discrete subunits[17,18] but this situation falls well short of what happens in natural systems where EET over hundreds, if not thousands, of chromophores is commonplace. It seems doubtful that the same type of distributive patterns can be achieved by way of covalent chemistry and alternative ways to self-assemble artificial photon concentrators are needed. One such approach might be to make use of crystals containing regular arrangements of fluorophores held in such a way that self-quenching and self-absorption are kept to a minimum.[19] In principle, these photonic crystals could be capable of unusually long-range exciton migration and subsequent trapping on a length scale comparable to that of the natural systems. Here, we describe a simple prototype that displays most of the desirable features, critically being able to operate efficiently in the solid state, but harvests only a modest fraction of the solar spectrum. The main objective of this study is to devise a simple means for self-assembly of a system displaying extended exciton migration but with the capacity to trap the excitons in the form of long-lived emission.

Results and Discussion

The molecular formula of the target compound MBIC is shown as Figure 1. Samples of MBIC were prepared[20] by amination of the corresponding naphthalic anhydride and crystallized from

[a] R. Al-Aqar, Dr. A. Atahan, Prof. Dr. A.C. Benniston, T. Perks, Prof. Dr. A. Harriman
Molecular Photonics Laboratory, School of Chemistry, Bedson Building
Newcastle University, Newcastle upon Tyne, NE1 7RU, United Kingdom
E-mail: anthony.harriman@ncl.ac.uk
[b] Dr. A. Atahan
Department of Polymer Engineering, Faculty of Technology, Duzce University
Duzce 81620, Turkey
[c] Dr. P. G. Waddell
Crystallography Laboratory, School of Chemistry, Bedson Building
Newcastle University, Newcastle upon Tyne, NE1 7RU, United Kingdom

Supporting information for this article is given via a link at the end of the document.

mixtures of chloroform and hexane. The same crystal packing was evident from multiple batches. However, recrystallization from acetic acid gave rise to a different crystal packing (i.e., a polymorph). In both cases, no solvent molecules could be detected in the crystal structure. Here, we use only the former method for obtaining crystals. Full experimental details are provided as part of the Supporting Information, together with analytical data for the compound. It might be noted that, although individual molecules of MBIC are polar (computed dipole moment = 21.6 D) to such a degree that it dissolves slightly in water, the crystal is non-conducting as demonstrated by single-crystal electronic conductivity measurements. This finding is important because it helps to eliminate the possibility of long-range electronic interactions between adjacent molecules in the crystal.

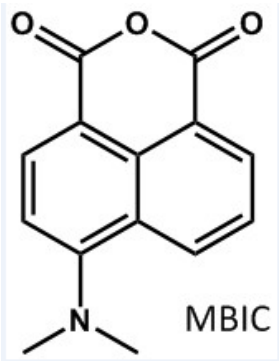

Figure 1. Molecular formula for the target compound MBIC.

In fluid solution, the target compound MBIC displays the optical properties considered characteristic of an intramolecular charge-transfer state.[21,22] Thus, the absorption band associated with the lowest-energy transition is relatively broad and featureless; in chloroform, the molar absorption coefficient at the band maximum (λ_{MAX}) of 420 nm is 10,720 M^{-1} cm^{-1} while the oscillator strength for the entire transition is 0.20. The absorption maximum shifts towards lower energy with increasing dielectric constant of the solvent but there is no change in the band shape (see Supporting Information). Fluorescence is readily detected in fluid solution and again the emission band is quite broad and essentially featureless. An exception to this generality occurs with nonpolar solvents, such as cyclohexane, where the fluorescence spectrum is slightly structured. The emission maximum (λ_{FLU}) moves steadily towards lower energy with increasing polarity of the solvent, measured crudely in terms of the static dielectric constant (ε_S), while the Stokes' shift increases progressively during this change. Analysis of the Stokes' shift in terms of the Lippert-Mataga expression[23] indicates that the dipole moment of the excited-singlet state exceeds that of the ground state by around 5 D. In turn, quantum chemical calculations made at the DFT level (B3LYP/aug-cc-pVTZ) are consistent with a ground-state dipole moment of 21.6 D. For the corresponding excited-singlet state, the dipole moment is computed by TD-DFT to be 26.5 D, the difference between ground- and excited-state values being in remarkable accord with experiment. In all solvents, there is good agreement between excitation and absorption spectra while time-resolved emission profiles were mono-exponential.

The fluorescence quantum yield (Φ_F) varies over a wide range and decreases with increasing solvent polarity (Table 1). Likewise, the excited-state lifetime (τ_S) decreases from 10 ± 0.2 ns in cyclohexane to 0.25 ± 0.05 ns in acetonitrile. There is a corresponding decrease in the radiative rate constant (k_{RAD}) with increasing solvent polarity. Such behavior is highly characteristic of organic molecules exhibiting strong intramolecular charge-transfer interactions.[24] In deoxygenated 2-methyltetrahydrofuran (2-MTHF) solution, laser flash photolysis studies indicate transient formation of the triplet-excited state. This species shows weak absorption centered at around 360 nm and decays via exponential kinetics with a lifetime of 25 ± 5 μs. Confirmation of triplet formation was obtained by the observation of strong phosphorescence at 550 nm in a 2-MTHF glass at 77K containing 20% v/v iodomethane. The latter spectrum shows none of the characteristics expected for an intramolecular charge-transfer state but is similar to that anticipated for a π,π* excited state.[25] Cyclic voltammetry studies made in acetonitrile solution show that MBIC undergoes one-electron, quasi-reversible reduction with a half-wave potential of -1.66 V vs SCE. Under the same conditions, one-electron oxidation is electrochemically irreversible and occurs with an oxidative peak potential of 0.85 V vs SCE. The energy of the charge-transfer state in acetonitrile solution is roughly 2.60 eV, compared to that of the excited-triplet state of 2.25 eV, such that intersystem-crossing[26] might be expected to compete with charge recombination fluorescence in fluid solution.

Table 1. Summary of the photophysical properties determined for MBIC in a range of organic solvents at room temperature.

Solvent	ε_S [a]	λ_{MAX} / nm	λ_{FLU} / nm	Φ_F	τ_S / ns	k_{RAD} / 10^7 s^{-1} [b]
Cyclohexane	2.02	392	465	1.00	10.5	9.5
Benzene	2.27	409	503	0.95	10.6	9.0
1,4-Dioxane	2.27	405	514	0.67	8.7	7.7
Toluene	2.43	407	502	0.87	10.3	8.5
Dibutyl ether	3.18	399	494	0.90	9.5	9.5
Diethyl ether	4.42	403	0.85	0.95	8.2	10.0
Chloroform	4.89	420	509	0.63	7.3	8.6
Butyl acetate	5.01	409	517	0.30	4.1	7.3
Chlorobenzene	5.74	418	510	0.13	2.7	4.8
Propyl acetate	6.00	410	519	0.066	1.5	4.4
Ethyl acetate	6.03	412	522	0.057	1.4	4.1
2-MTHF [c]	6.97	409	515	0.088	1.8	4.9
THF [d]	7.47	414	524	0.075	1.5	5.0
Dichloromethane	8.93	423	519	0.040	0.80	5.0
Octanol	10.30	418	533	0.055	0.88	6.3
1,2-DCE [e]	10.74	424	524	0.023	0.75	3.1
Butan-1-ol	17.5	422	540	0.020	0.67	3.0
Acetone	21.36	419	536	0.0055	0.55	1.0
Ethanol	24.5	416	550	0.012	0.64	1.9
Butyronitrile	24.56	422	538	0.016	0.72	2.2
Propionitrile	28.86	422	540	0.012	0.48	2.5
Methanol	32.7	422	542	0.010	0.40	2.5
Acetonitrile	35.94	425	545	0.0055	0.25	2.2
DMF [f]	37.06	428	550	0.0040	0.17	2.4
PC [g]	62.93	428	555	0.0035	0.18	1.9

(a) Static dielectric constant, taken from literature compilations. (b) Radiative rate constant. (c) 2-Methyltetrahydrofuran. (d) Tetrahydrofuran. (e) 1,2-Dichloroethane. (f) N,N-Dimethylformamide. (g) Propylene carbonate.

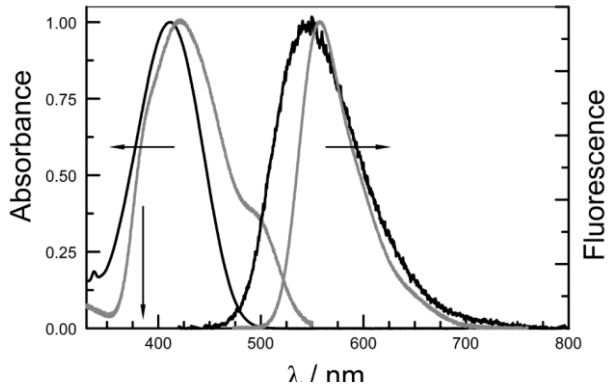

Figure 2. Comparison of the absorption and fluorescence spectra recorded for MBIC in ethanol solution (black curve) and for a single crystal of MBIC (grey curve) at room temperature. The vertical arrow represents the excitation wavelength used for emission studies.

Quite similar absorption and fluorescence spectral profiles are observed from a single crystal of MBIC at room temperature when illuminated at 385 nm (Figure 2). The absorption spectrum for the crystalline sample remains similar to that found in solution, in particular the strong intramolecular charge-transfer character is clearly evident, but a lower-energy band is seen at around 500 nm. This latter transition might be associated with Frenkel excitons,[27] which are often apparent with crystalline materials.[28] Charge-recombination fluorescence can be observed for the crystal, with a maximum centered at 557 nm. Relative to MBIC in solution, the emission profile recorded for the crystal is slightly narrower. This could be because of the absence of solvent stabilization. The fluorescence profile remains unchanged for a variety of excitation wavelengths but the spectral maximum is red-shifted compared to even the most polar solvents. Furthermore, dispersing crystals of MBIC in dried KBr powder, followed by pressing into a compact disc, gives rise to a similar spectrum. Indeed, the same profile is obtained from filter paper impregnated with micro-crystals of MBIC.

The conclusion, therefore, is that MBIC emits charge-recombination fluorescence in the crystalline phase. While not unique,[29,30] this behavior is uncommon and attests to the fact that MBIC does not undergo substantial self-quenching in the solid matrix. A temperature dependence emission study carried out with a single crystal of MBIC indicates that the re-organization energy associated with charge-recombination is ca. 1,530 cm^{-1} while the Huang-Rhys factor[31] is 0.50. The latter is fully consistent with the exciton being localized on a single molecule,[32] rather than being spread over several aligned molecules within the lattice. The re-organization energy and Huang-Rhys factor are small compared to typical values determined in solution but, as mentioned above, solvent stabilization is not possible in the crystal. The emission peak maximum does not change significantly (i.e., <5 nm) over a temperature variation from 20 to 200 ^{0}C.

The crystal structure exhibits stacking of the molecules via π-π interactions along the crystallographic [100] direction (a-axis). Molecules in the stack are arranged disk-like with a head-to-head orientation and are hence related to each other by a pure translation along the direction of the stack (Figure 3). A typical needle-like crystal of MBIC has a crystallographic density of 1.50 g/cm^3. It is interesting to note that the alternative crystal structure, obtained by crystallization from acetic acid, has the MBIC molecules arranged in a head-to-tail fashion (Figure 4). This is a remarkable variation in crystal structure, being caused solely by a change in the crystallizing medium, which is far from common in the field. It might be anticipated that, given the high molecular polarity of MBIC, the two morphologies will be subjected to quite disparate intermolecular dipole-dipole interactions. This, in turn, could lead to an unusual way to manipulate non-linear optical properties of the material.

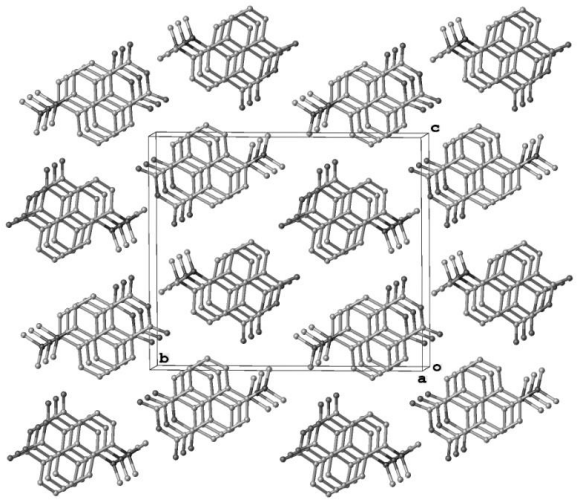

Figure 3. Crystal packing diagram determined for MBIC. The same packing is found after crystallization in the presence of Rh-B. A photograph showing the crystal dimensions is provided as part of the Supporting Information.

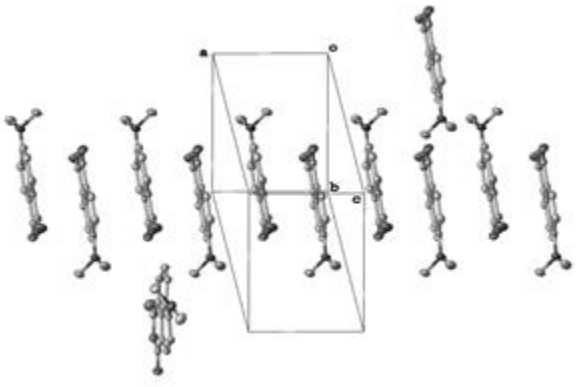

Figure 4. Crystal packing diagram for the second polymorph of MBIC, as obtained by recrystallization from acetic acid.

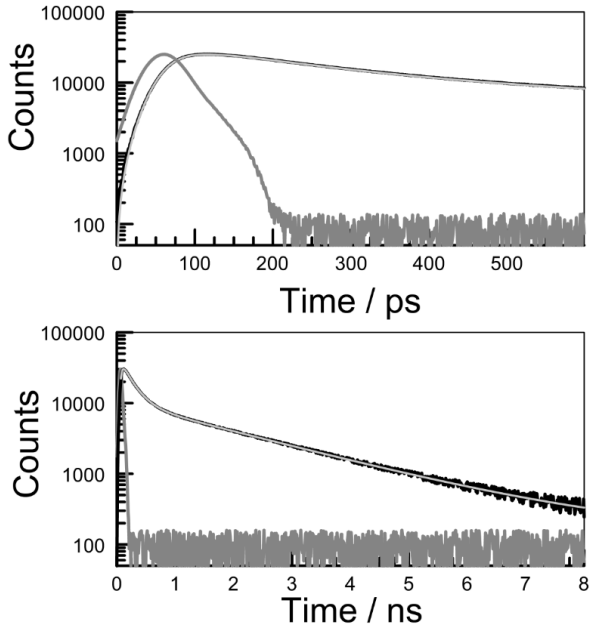

Figure 5. Examples of time-resolved fluorescence decay curves recorded for a single crystal of MBIC at room temperature. The curves refer to two different time bases. The instrument response function is shown as a grey curve while the best fit to a two-exponential decay process is shown as a light-grey curve running through the data points (black curve).

The emission quantum yield determined for a single crystal of MBIC using an integrating sphere was found to be 0.09. This is similar to the value expected for MBIC in a weakly polar environment, such as that provided by 2-MTHF. Time-resolved fluorescence studies following excitation at 370 nm with a short-duration (FWHM = 90 ps), pulsed LED are consistent with dual-exponential decay kinetics. The recovered lifetimes are 0.20 ± 0.08 ns (80%) and 2.0 ± 0.08 ns (20%). The fractional components do not change significantly with detection wavelength (see Supporting Information), at least over a modest range, and are independent of excitation wavelength. The longer lifetime was recovered reproducibly for different time ranges, count rates and total signal intensity. This was not the case for the short lifetime, which proved difficult to reproduce consistently, but its fractional contribution to the total signal remained around 80%. It appears that the shorter lifetime refers to a distribution of lifetimes having a mean value of around 0.2 ns. Indeed, the convoluted decay profiles could be simulated using the maximum entropy method[33] (MEM), together with the instrumental response function, to indicate a Gaussian-shaped distribution of lifetimes centered at 0.2 ns and with a variance of ±0.05 ns together with a single lifetime of 2.0 ns. An example of this fitting routine is shown as Figure 6. The MEM analysis appears more robust than the dual-exponential model when considered over a range of time bases, although the latter gives acceptable statistical fits on a single time base.

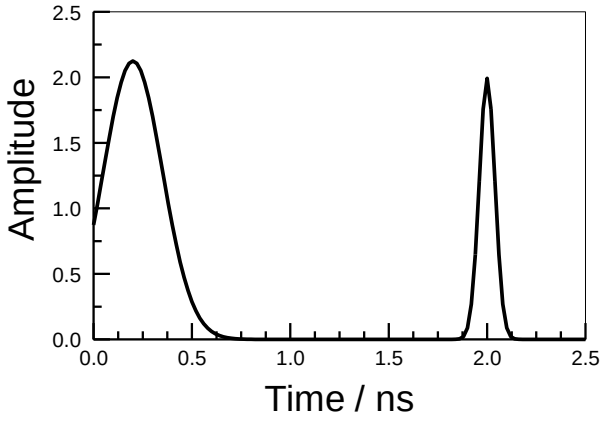

Figure 6. Maximum entropy method analysis of the time-resolved emission profile for a single crystal of MBIC. The analysis corresponds to a distribution of lifetimes centered at 0.2 ns and a single lifetime of 2.0 ns.

Our interpretation of this behavior is that the crystal comprises MBIC molecules in two distinct environments. Since there are no obvious lattice irregularities, these two disparate localities most likely refer to bulk- and surface-bound molecules. On the basis that the longer lifetime (i.e., the smaller contribution) refers to surface states and that the radiative lifetime remains fixed for crystalline samples, it appears that most (i.e., ca. 75%) of the steady-state emission is associated with the surface. The occurrence of dual-exponential decay processes was recognized earlier for certain emissive quantum dots.[34,35] Here, exciton migration occurs within the interior but the exciton becomes trapped as it approaches the surface, with the resultant surface-states decaying relatively slowly. We might anticipate comparable behavior for crystalline MBIC.

It was not possible to grow larger crystals of MBIC where the relative concentration of surface-bound material might be reduced. Polishing the crystals with SiC ribbon (9 micron) led to a modest reduction in the relative contribution of the longer-lived component (i.e., from 20% to 12% on average) while grinding the wet crystals before drying gave the opposite effect. Here, the fractional contribution of the longer-lived component increased to around 30% on average. Dissolving the surface layer in hot water resulted in a similar increase in the fractional contribution of the longer-lived species. These various qualitative studies are taken to be consistent with an amorphous layer of MBIC molecules associated with the surface of the crystal. The amorphous region is believed to be responsible for the longer emission lifetime.

Analysis of the X-ray structure denotes that the center-to-center separation between MBIC molecules aligned along the stack is only 3.8 Å. In contrast, the closest center-to-center distances between molecules in adjacent stacks are 9.0 and 9.75 Å (see Supporting Information for details). Because of the large Stokes' shift induced by the strong charge-transfer character, the spectral overlap integral (J_{DA} = 3.25 x 10^{-5} cm) for Förster-style

excitation energy migration between neighboring MBIC molecules is relatively small.[36] Likewise, the transition dipole moment calculated[37] for MBIC in solution, computed to be 1.53 D, is kept modest by the weak oscillator strength. Nonetheless, this is offset to a large extent by the short separation distance and good dipole-dipole alignment between adjacent MBIC molecules in the stack. Indeed, it can be calculated[38] that the hopping time between stacked molecules is on the order of 0.3 ps (see Supporting Information for details). Taking the shorter of the two lifetimes as reflecting the bulk molecules, we can estimate that, on average, 50% of the excitons will undergo at least 400 hops before returning to the ground state while 10% will make at least 1,400 hops. Of course, any such migration will be incoherent and it should be stressed that the Coulombic mechanism[39] usually underestimates the hopping time at very short separations.[40] The mean time needed for an exciton to cross between stacks is 50 ± 8 ps. Thus, an exciton has only ca. 1% chance to pass to a nearby stack rather than migrate to the neighboring MBIC molecule along the same stack but, within its lifetime, we might expect the exciton to make at least four trans-stack jumps. Our observation that the shorter-lived species shows a distribution of survival times seems fully consistent with a variety of trapping rates reflecting the distance travelled prior to arrival at the surface states.

In passing, it might be noted that the second polymorph exhibits a similar fluorescence spectrum to that shown as part of Figure 2, with a comparable quantum yield of 0.11. Again, time-resolved emission spectroscopy indicates dual-exponential kinetics, with global lifetimes of 0.58 ± 0.07 (88%) and 2.2 ± 0.1 ns (12%) being recovered. The distance between adjacent MBIC molecules in the aligned stacks is enlarged slightly to 4.0 Å. On the basis of the same analysis as applied above, the hopping time for excitons associated with a particular head-to-tail stack is 0.4 ps, this being somewhat longer than that for the corresponding head-to-head stack. It would appear that the head-to-tail structure has a slightly more extended surface layer, this being responsible for around 3% of the total crystal. More importantly, the lifetime attributed to bulk MBIC molecules is considerably longer than that found for the head-to-head arrangement. It is difficult to be precise about the origin of this effect other than to note that the photophysics of MBIC are highly sensitive to the local environment. Thus, dipole-dipole interactions within the crystal seem to contribute towards the factors influencing the photophysics of the charge-transfer state. This type of behavior is likely to be restricted to strongly dipolar molecules.

The calculated hopping rates are derived[38] from conventional Förster theory for electronic energy transfer in the weak coupling limit. It might be argued[39,40] that this treatment is inadequate for exciton hopping in the crystalline phase, especially given the apparent involvement of Frenkel excitons and their possible interaction with the charge-transfer state.[27] We are unable to measure the hopping times by direct experiment but the close proximity and alignment of MBIQ molecules should ensure rapid exciton migration along the stack. This is the important point and the proposed hopping rates should be taken with caution.

In separate experiments, MBIC was crystallized in the presence of a very small amount of Rhodamine B (Rh-B). The latter was chosen because, in solution phase, its absorption spectrum overlaps the emission profile of MBIC, it shows intense fluorescence and it has a flat shape not too dissimilar from that of MBIC. It was anticipated that Rh-B might intercalate into the MBIC stacks within the crystal. Indeed, the presence of Rh-B at very low doping levels does not perturb the crystal structure of MBIC as determined by X-ray crystallography but these studies did not define the location of the dopant. Likewise, the precise level of loading could not be defined although absorption spectroscopy carried out with dissolved crystals indicated that this was similar to that of the mixture before crystallization. The presence of Rh-B has no noticeable effect on the dimensions or color of the crystal but does affect the emission spectral profile. At the very low loadings used here, it was not possible to detect Rh-B by optical absorption spectroscopy while the excitation spectrum recorded for emission associated with bound Rh-B corresponded to the absorption spectrum of crystalline MBIC. Washing the doped crystal with cold water before drying with warm N_2 serves the purpose of removing the fluorescence due to Rh-B. Under these conditions, the crystal remains intact and emits as described earlier while the aqueous solution shows characteristic fluorescence from Rh-B. The impression, therefore, is that Rh-B is associated with surface-states of the emerging crystal rather than occupying a site within the MBIC stacks.

In ethanol solution, Rh-B exhibits sharp absorption (λ_{MAX} = 545 nm) and fluorescence (λ_{FLU} = 563 nm) spectra (see Supporting Information). The emission lifetime (τ_S) decreases with increasing concentration, as does the quantum yield, but reaches an upper limit of 2.8 ns at micro-molar concentrations. It has been reported that the absorption spectrum remains essentially unchanged[41] when Rh-B is adsorbed at sub-monolayer coverage onto ZnO crystals. In contrast, adsorption of Rh-B from water onto a quartz plate causes a modest red shift[42] for both absorption (λ_{MAX} = 558 nm) and emission (λ_{FLU} = 576 nm) maxima while τ_S increases to 3.1 ns (see Supporting Information). Adsorption of Rh-B from aqueous solution onto the outer surface of a MBIC crystal gives rise to a broad fluorescence spectrum superimposed over the usual emission profile characterised for MBIC (see Supporting Information). This broad spectrum, the maximum for which moves progressively towards the blue with increasing contact time between Rh-B solution and the MBIC crystal, is assigned to aggregated dye on the surface of the crystal.[43] We can now compare these spectra with that observed for the Rh-B doped MBIC crystals prepared by growing in the presence of dye.

Thus, doped crystals were illuminated at 385 nm, where Rh-B is unlikely to contribute to the absorption profile, especially at the concentration used (see Supporting Information). The resultant fluorescence spectrum differs, albeit slightly, from that characterized for crystalline MBIC (Figure 7). In fact, the new spectrum can be reproduced reasonably well by a mixture of emission profiles for crystalline MBIC and for Rh-B adsorbed onto a quartz plate (Figure 7). For example, at a Rh-B loading of 5 mpm (i.e., 10 mols of Rh-B per million mols of MBIC or a molar ratio of 100,000 in favor of MBIC), the emission spectrum is nicely reproduced by allowing for 40% MBIC and 60% Rh-B (Figure 7). Furthermore, exact agreement between compiled and observed fluorescence spectra can be reached by slight shifting (i.e., 2-3 nm) of the Rh-B maximum wavelength but retaining an equivalent

profile. The same situation is found for other loadings of Rh-B; in each case the observed spectrum being a supposition of individual spectra assigned to MBIC and Rh-B. Iterative reconstruction procedures based on global analysis data fitting with Levenberg-Marquardt methods[44] and assuming a two-component mixture allowed the fractional contribution (α) of Rh-B emission to the total spectrum to be determined (Table 2). It can be seen that there is a smooth correlation between α and the initial doping level, although saturation seems to occur at the higher loadings. Since direct excitation of Rh-B can be eliminated, the only reasonable explanation for these mixed spectra involves electronic energy transfer (EET) from MBIC to Rh-B occurring in the solid matrix.[45]

Table 2. Emission properties recovered for the crystals of MBIC loaded with a minor amount of Rh-B.

Property	S0 [(a)]	S1	S2	S3	S4
Rh-B / mpm[(b)]	0	2.5	5	10	15
Φ_F	0.09	0.092	0.115	0.132	0.123
α / % [(c)]	0	35	60	75	65
τ_1 (A_1) / ps	0.20 (79.8)	0.14 (82.5)	0.18 (81.6)	0.10 (74.3)	0.18 (78.3)
τ_2 (A_2) / ns	2.00 (20.2)	1.75 (13.7)	1.25 (10.3)	1.00 (14.7)	0.95 (12.4)
τ_3 (A_3) / ns	NA	5.3 (3.8)	5.4 (8.1)	5.4 (11.0)	5.4 (9.3)

(a) Refers to sample number. Each sample size was 200 mg and each measurement was repeated ten times. (b) Loading of Rh-B expressed in terms of mols and converted to mols Rh-B per million mols of MBIC. (c) Fraction of emission yield assigned to Rh-B on the basis of spectral deconstruction into two overlapping spectra. (d) Excited-state lifetimes derived from the time-resolved emission decay curves following excitation at 370 nm. The fractional contribution at 575 nm, A, is given in parenthesis. For τ_1, the quoted value is the mean of the distribution obtained from MEM analysis.

For the same samples, time-resolved fluorescence decay profiles required analysis as the sum of three-exponential terms (Figure 7); such analysis has to be undertaken with caution![46] However, in the present case, a logical account of the complex kinetics could be reached as follows: One lifetime (τ_3) was found to be 5.4 ± 0.1 ns, which is somewhat longer than that (τ_S = 3-4 ns) determined for Rh-B in a small range of solid samples.[42] Furthermore, the fractional amplitude (A_3) for this particular component increased with increasing loading of Rh-B, until attaining a saturation level (Table 2). Thus, we assign the longest-lived component to emission from Rh-B, which we believe to be predominantly associated with the surface structure of the crystal. Support for this identification is nicely derived by comparison of time-resolved emission profiles recorded at early (i.e., 0.4-0.5 ns) and late (i.e., 4-5 ns) gate times after the excitation pulse (Figure 8). The early-gated spectrum resembles emission characteristic of the MBIC crystal while the late-gated profile closely resembles the spectrum recorded for Rh-B adsorbed onto quartz at sub-monolayer coverage.

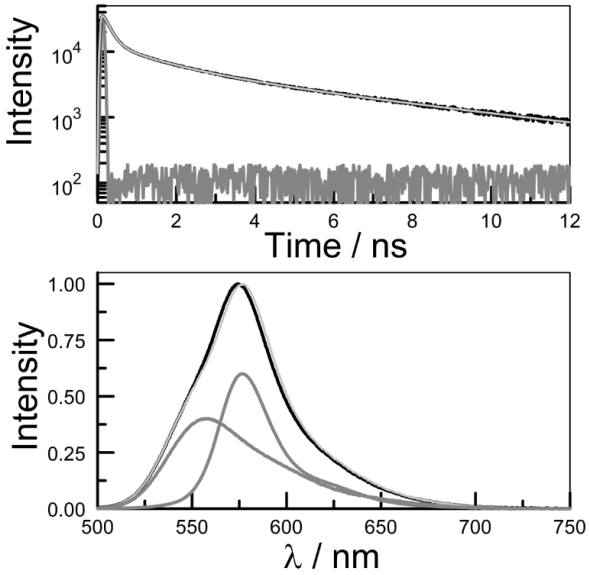

Figure 7. The lower panel shows the fluorescence spectrum recorded for a crystal of MBIC doped with Rh-B, at a loading of 5 mpm, (black curve) and the reconstruction (light-grey curve) from components associated with crystalline MBIC (grey curve) and Rh-B adsorbed onto a quartz plate at sub-monolayer coverage (grey curve). The upper panel shows the time-resolved fluorescence decay profile recorded at 575 nm with the instrumental response function in grey, the experimental data as a black curve and the fit to the sum of three exponentials as a red curve.

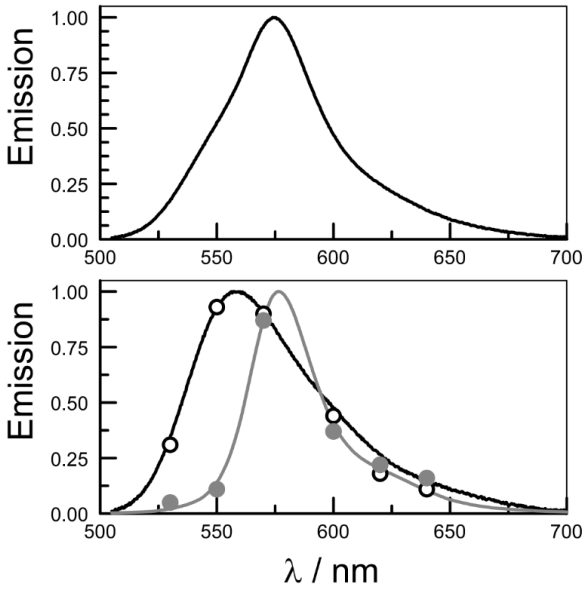

Figure 8. The upper panel shows the emission profile recorded for a single crystal of MBIC doped with Rh-B at a level of 5 mpm. The lower panel shows normalized time-resolved emission spectra recorded at 0.4-0.5 ns (open circles) and 4-5 ns (filled circles) gate times. The solid lines correspond to simulated spectra for pure MBIC (black curve) and a mixture of (15%) MBIC and (85%) Rh-B (grey curve).

The shortest lifetime (τ_1) shows the largest fractional contribution (A_1) and remains closely comparable to that assigned to MBIC molecules comprising aligned stacks within the interior of the crystal. As before, it proved difficult to obtain unique solutions for this lifetime when varying the count rate or the total signal accumulation. This behavior is considered characteristic of a distribution of lifetimes[47] and is better reflected by the MEM analysis.[48] Fast exciton hoping between neighboring MBIC molecules and across stacks appears to be unaffected by the presence of Rh-B. Again, this seems in keeping with the suggestion that most of the Rh-B resides in an amorphous region near the surface of the crystal.

The remaining lifetime (τ_2) is the only one that varies from sample to sample, decreasing progressively with increasing loading of Rh-B (Table 2). The ratio of fractional contributions made by τ_1 and τ_2 remains reasonably constant across the series while the magnitude of τ_2 is not too far removed from that attributed to surface-localized MBIC in the pure crystal. On this basis, we assign τ_2 to MBIC molecules comprising the surface layer and attribute the shortening of the lifetime to EET to Rh-B molecules also localized at the surface. This leads to the overall scheme illustrated by Chart 1. Excitons generated within the interior of the crystal oscillate incoherently along the aligned stacks until approaching the surface states. Trapping occurs near to the surface so as to generate a longer-lived excited state of MBIC, presumably existing as a somewhat amorphous phase. Loading the MBIC crystal with Rh-B tends to localize the dopant at the surface, where it acts as an acceptor for excitons migrating slowly around the surface layer of MBIC. The model considers exciton trapping by surface-bound MBIC and surface-mediated EET to Rh-B to be irreversible steps.

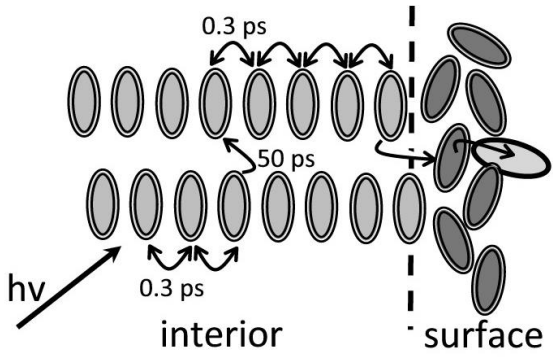

Chart 1. Pictorial representation of rapid exciton migration along and between stacks within the MBIC crystal (grey disk), followed by exciton trapping at surface-bound MBIC molecules (dark grey disk) and EET to the Rh-B dopant (light-grey disk with dark surround).

On the basis of this model, fluorescence from Rh-B is the consequence of energy migration within the MBIC stacks, trapping by surface-bound MBIC molecules and EET to ground-state Rh-B. The excitation spectrum recorded at an emission wavelength where Rh-B is expected to dominate the fluorescence profile, namely 580 nm (Figure 7), corresponds to absorption by MBIC but does not feature direct absorption by the dye. The time-resolved emission spectra recorded at early and late time gates provide further support for the notion that Rh-B fluorescence arises from secondary events. Using this information, it becomes clear that the derived lifetime of 5.4 ns for the Rh-B dopant is too long. Convolution of τ_3 with an exponential function with a lifetime corresponding to τ_2, shortens the effective singlet-state lifetime of the dye to around 4 ns. This brings it more into expectation with an isolated Rh-B molecule in the solid state.

Even at the very low loadings of Rh-B employed here, there is the impression that saturation has been reached in as much as both the total emission and the fractional contribution attributed to Rh-B reach a maximum at around 10 mpm (Table 2). It is likely that self-association of Rh-B, or self-quenching, becomes important at the highest loading.[49] Under optimum conditions, about 50% of the MBIC fluorescence is quenched by the presence of a very low concentration of Rh-B. There is a compromise between increasing the level of quenching and avoiding self-association in the surface region but, under appropriate conditions, loading the crystal with Rh-B leads to a modest (i.e., ca. 50%) increase in the fluorescence quantum yield. This was not the case when Rh-B was replaced with Cresyl Violet;[50] here, there was no indication for association of the dye with the MBIC crystal and no EET from MBIC to Cresyl Violet.

The concept of multiple, linear EET events followed by trapping at a terminal is not new and was introduced successfully by Calzaferri[51] in the form of doped zeolites. Related theoretical studies[52,53] have developed Monte-Carlo modelling algorithms to describe exciton migration and trapping in crystals and on the outer surfaces of micro-heterogeneous media.[54] Similar, but more spatially restricted, processes are known to occur with certain dendrimers[55] and organic clusters.[56,57] Of course, exciton migration in photosynthetic light-harvesting antennae has been subjected to considerable experimental[58] and theoretical[59] investigation over many decades. For crystalline MBIC, our illumination studies were carried out at low irradiance such that only a single exciton is present on the crystal at any given moment. Allowing for a common radiative rate constant for both bulk and surface-bound MBIC, we can estimate that the latter accounts for about 2% of the total MBIC.

A typical Rh-B loaded crystal has dimensions of 2 x 0.2 x 0.2 mm (see Supporting Information), which corresponds to a total volume of 8×10^{-5} cm^3. With a crystallographic density of 1.50 g/cm^3, the same crystal contains roughly 3×10^{17} molecules of MBIC. Now, we can estimate that the so-called surface layer comprises 6×10^{15} molecules of MBIC. At an Rh-B loading of 10 mpm, and assuming localization in the surface layer, we can estimate the concentration of dopant as being 500 mpm. This remains a very low level. Indeed, the critical distance for Förster-type EET from MBIC to Rh-B was calculated[60] as being 12.5 Å, on the basis of random orientation. Given the low dopant concentration, it seems likely that fast exciton migration must occur between MBIC molecules in the surface layer before trapping by the embedded dye molecule.

Now, the computed molecular volume for MBIC is 237.74 Å^3. In the limit of non-random distribution within the surface layer, the

average distance between MBIC molecules should be 6 Å while the distance between Rh-B molecules would be 72 Å at a loading of 10 mpm. The likelihood, therefore, is that up to twelve molecules of MBIC are interspersed between nearest Rh-B molecules within the surface layer. This means that incoherent exciton migration must occur among surface-bound MBIC molecules until the exciton approaches to within a certain distance of the embedded Rh-B acceptor. With 6 Å separation of MBIC molecules, the hopping time for surface-bound MBIC excitons would be 28 ps. These crude values seem self-consistent with the proposed mechanism, but need to be considered in terms of reservations about the validity of Förster theory under such conditions.

Crystals of MBIC loaded with Rh-B were incorporated into a clear, polyester film so as to form a photonic membrane. Excitation of the film at 385 nm results in the appearance of fluorescence from the crystal that closely resembles the profile recorded separately for an isolated single crystal. Thus, dispersing the co-crystal in the fluid monomer prior to polymerization does not degrade the crystal or extract Rh-B from the surface. Now, we have a simple means to extend the surface area of the light-harvesting array without introducing large regions of optical transparency. The membrane was used to sensitize an amorphous silicon solar cell, although emission from Rh-B is far from ideal for this purpose. At low concentration, performance of the doped crystal is inferior to that of a membrane formed from Rh-B but the latter suffers badly from self-absorption at higher concentrations. Furthermore, the membrane formed from pure Rh-B undergoes fast photo-degradation whereas the performance of the doped crystal-derived membrane does not degrade over prolonged illumination times. Its performance is vastly (i.e., 40-times) better than similar membranes formed from planar dyes such as perylene that undergo both self-absorption and aggregation.

Conclusions

In conclusion, we have described a new type of photonic crystal that might have useful applications in the field of photon concentrators. By making use of an intramolecular charge-transfer system, we ensure a substantial Stokes' shift which minimizes self-absorption. The effective Stokes' shift is further extended by way of EET to the dopant, present at very low concentrations. By growing the crystal in the presence of dopant, as opposed to coating the surface of a fully grown crystal with dye, it becomes possible to increase the loading without aggregation. Even so, saturation is reached at a relatively low concentration of dopant. A further drawback of the present system concerns the modest spectral overlap integral[61] between absorption by Rh-B and emission from MBIC. This term needs to be increased markedly in order to optimize exciton trapping by the dopant. A promising outlet for this prototype is the fabrication of artificial membranes by embedding crystals in a thin plastic film. This offers a route for exciton transfer between crystals, thereby providing directionality and further lowering the dopant level. Studies are underway aimed at optimizing the performance of the membrane as a sensitizer for organic solar cells and photoredox reactions.

An interesting aside relates to the remarkable observation that the alignment of MBIC molecules within the stack can be switched between head-to-head and head-to-tail geometries (Figures 3 and 4) simply by changing the crystallizing medium. This alignment must affect dipole-dipole,[62] and indeed dipole-quadrupole, interactions within the crystal. Such interactions are of considerable importance in determining rates of Förster-type EET[63] and have been implicated in both quantum information processing[64] and the development of dipole lasers.[65] There have been no prior attempts to manipulate the properties of photonic crystals by way of perturbing dipole-dipole interactions but our work has shown that this might be feasible. We do see a difference in the time-resolved emission parameters derived for the two structures, with the head-to-tail alignment giving a more substantial surface layer that is less well coupled to the aligned stacks. Additional work is needed to examine the significance of this dipole switching in terms of opto-electronic properties.

Experimental Section

Full synthetic details[20] are provided as part of the Supporting Information, including analytical data for MBIC. Solvents were spectroscopic grade, checked for fluorescent impurities before use, from commercial sources. Cyclic voltammetry was carried out with MBIC (2 mM) dissolved in de-aerated, anhydrous acetonitrile containing tetra-N-butyl ammonium hexa-fluorophosphate (0.2 M) as background electrolyte. The working electrode was a glassy carbon disk and the counter electrode was a Pt wire. The SCE reference electrode was calibrated with respect to ferrocene as an internal standard. Absorption spectra were recorded with a Hitachi U-3310 spectrophotometer while emission spectra were recorded with a Hitachi F-4500 spectrophotometer. Solution-phase emission studies were made with optically dilute solutions and quantum yields were recorded relative to perylene in cyclohexane[66] as reference. Fluorescence lifetimes were measured by time-correlated, single photon counting methods, with excitation at 370 nm using a short-duration (FHWM = 90 ps) laser diode. Data analysis was made using standard statistical protocols.[67]

Various methods were used to prepare solid samples for fluorescence spectroscopy. Single crystals were mounted on a rod and positioned carefully inside the sample chamber of the instrument. Samples of MBIC were ground with an excess of KBr and pressed into a pellet. Crystals were mixed gently onto a filter paper support so as to impregnate the paper with tiny crystals. Quantitative measurements were carried out using an integrating sphere. Temperature dependent studies were made with the sample housed in a Harricks TFC-M25 demountable liquid cell. To extract Rh-B from the doped crystals, an aliquot of crystals was placed on a glass frit and washed with cold water. Washing was continued until the extract was no longer fluorescent. Surface loading of Rh-B onto glass or quartz slides was achieved as reported earlier.[41] Artificial membranes were prepared by packing crystals into a Teflon template of various dimensions. The

template was located on a Teflon plate to ensure easy removal of the dried membrane. Casting resin (Easy Composites Ltd.), pre-treated with activator, was poured gently over the crystals and allowed to set for 48 hours in the dark. After drying the edges were polished with fresh cotton. The resultant disk, usually circular with diameter of 2 cm, was inserted into a slot machined into a Teflon holder used to house a silicon solar cell (Conrad 19-12-81, 0.5V, 400 mA). The disk was illuminated with a 250W solar illuminator fitted with optical fibre and defocussing lens.

Crystal structure data were collected on an Xcalibur, Atlas, Gemini ultra-diffractometer equipped with an Oxford Cryosystems CryostreamPlus open-flow N_2 cooling device, using an Enhance Ultra (Cu) X-ray Source (λ CuKα = 1.54184 Å) for the head-to-head geometry and Enhance (Mo) X-ray Source (λ MoKα = 0.71073 Å) for the head-to-tail geometry. Cell refinement, data collection and data reduction were undertaken via CrysAlisPro (Agilent Technologies, Version 1.171.36.32). Intensities for the head-to-tail geometry were corrected for absorption in an analytical numerical fashion using a multifaceted crystal model based on expressions derived by Clark and Reid,[68] whereas for the head-to-head geometry an empirical absorption correction using spherical harmonics was implemented through the Olex2 interface.[69] The structure of the head-to-head geometry was refined as a 2-component twin.

Acknowledgement

We thank Newcastle University for financial support of this work. AA gratefully acknowledges the award of a research scholarship from TUBITAK (The Scientific and Technological Research Council of Turkey) while RAA is endebted to The Higher Committee for Education Development in Iraq (HCED) for the award of a postgraduate studentship.

Keywords: electronic energy transfer • light harvesting • photophysics • fluorescence • polymorph

[1] G. McDermott, S. M. Prince, A. A. Freer, A. M. Hawthornthwaite-Lawless, M. Z. Papiz, R. J. Cogdell, N. W. Isaacs, *Nature* **1995**, *374*, 517-521.

[2] P. Horton, A. V. Ruban, R. G. Walters, *Ann. Rev. Plant Physiol. Plant Mol. Biol*. **1996**, *47*, 655-684.

[3] V. Sundstrom, T. Pullerits, R. van Grondelle, *J. Phys. Chem. B* **1999**, *103*, 2327-2346.

[4] a) O. Beja, M. T. Suzuki, J. F. Heidelberg, W. C. Nelson, C. M. Preston, T. Hamada, J. A. Eisen, C. M. Fraser, E. F. De Long, *Nature* **2002**, *415*, 630-633: b) R. A. Niederman, *Biochim. Biophys. Acta Bioenergetics* **2016**, *1857*, 232-246.

[5] a) Y.-C. Cheng, G. R. Fleming, *Ann. Rev. Phys. Chem*. **2009**, *60*, 241-262: b) R. J. Cogdell, H. Hashimoto, A. T. Gardiner, *Photosynth. Res*. **2004**, *80*, 173-179.

[6] M. Rudolf, S. V. Kimer, D. M. Guldi, *Chem. Soc. Rev*. **2016**, *45*, 612-630.

[7] a) L. P. Chen, P. Shenai, F. L. Zheng, A. Somoza, Y. Zhao, *Molecules* **2015**, *20*, 15224-15272: b) T. Roland, E. Heyer, L. Liu, A. Ruff, S. Ludwigs, R. Ziessel, S. Haacke, *J. Phys. Chem. C* **2014**, *118*, 24290-24301. b)

[8] R. Ziessel, A. Harriman, *Chem. Commun*. **2011**, *47*, 611-631.

[9] a) D. Gust, T. A. Moore, A. L. Moore, *Acc. Chem. Res*. **2001**, *34*, 40-48: b) D. Gust, T. A. Moore, A. L. Moore, *Acc. Chem. Res*. **2009**, *42*, 1890-1898.

[10] a) L. Hammarstrom, *Acc. Chem. Res*. **2015**, *48*, 840-850: b) Y. Tachibana, L. Vayssieres, J. R. Durrant, *Nature Photonics* **2012**, *6*, 511-518.

[11] A. C. Benniston, A. Harriman, *Mater. Today* **2008**, *11*, 26-34.

[12] A. Harriman, *Chem. Commun*. **2015**, *51*, 11745-11756.

[13] E. J. Alexy, J. M. Yuen, V. Chandrashaker, J. R. Diers, C. Kirmaier, D. F. Bocian, D. Holten, J. S. Lindsey, *Chem. Commun*. **2014**, *50*, 14512-14515.

[14] D. M. Guldi, *Chem. Soc. Rev*. **2002**, *31*, 22-36.

[15] M. R. Wasielewski, *J. Org. Chem*. **2006**, *71*, 5051-5066.

[16] J. Iehl, J.-F. Nierengarten, A. Harriman, T. Bura, R. Ziessel, *J. Am. Chem. Soc*. **2012**, *134*, 988-998.

[17] G. M. Hasselman, D. F. Watson, J. R. Stromberg, D. F. Bocian, D. Holten, J. S. Lindsey, G. J. Meyer, *J. Phys. Chem. B* **2006**, *110*, 25430-25440.

[18] R. Ziessel, G. Ulrich, A. Haefele, A. Harriman, *J. Am. Chem. Soc*. **2013**, *135*, 11330-11344.

[19] T. Sahin, M. A. Harris, P. Vairaprakash, D. M. Niedzwiedzki, V. Subramanian, A. P. Shreve, D. F. Bocian, D. Holten, J. S. Lindsey, *J. Phys. Chem. B* **2015**, *119*, 10231-10243.

[20] K. J. Kilpin, C. M. Clavel, F. Edafe, P. J. Dyson, *Organometallics* **2012**, *31*, 7031-7039.

[21] W. Schuddeboom, S. A. Jonker, J. M. Warman, U. Leinhos, K. A. Zachariasse, *J. Phys. Chem*. **1992**, *96*, 10809-10819.

[22] A. Harriman, M. Hissler, R. Ziessel, *Phys. Chem. Chem. Phys*. **1999**, *1*, 4203-4211.

[23] a) E. Lippert, *Z. Naturforsch* **1955**, *10A*, 541-545. b) N. Mataga, Y. Kaifu, M. Koizumi, *Bull. Chem. Soc. Jpn*. **1956**, *29*, 465-470.

[24] A. Brun, A. Harriman, Y. Tsuboi, T. Okada, N. Mataga, *J. Chem. Soc., Faraday Trans*. **1995**, *91*, 4047-4057.

[25] J. B. Birks, *Photophysics of Aromatic Molecules*, Wiley-Interscience, London, 1970.

[26] A. C. Benniston, A. Harriman, P. Li, J. P. Rostron, H. J. van Ramesdonk, M. M. Groenveld, H. Zhang, J. W. Verhoeven, *J. Am. Chem. Soc*. **2005**, *127*, 16054-16064.

[27] M. Hoffmann, K. Schmidt, T. Hasche, V. M. Agranovich, K. Leo, *Chem. Phys*. **2000**, *258*, 73-79.

[28] a) P.-A. Plötz, T. Niehaus, P. Kühn, *J. Chem. Phys*. **2014**, *140*, 174101. b) Y. Liao, V. Génot, R. Méallet-Renault, T. T. Vu, J.-F. Audibert, J.-P. Lemaistre, G. Clavier, P. Retailleau, R. B. Pansu, *Phys. Chem. Chem. Phys*. **2013**, *15*, 3186-3195.

[29] a) Y.-Q. Zhang, J.-X. Wang, Z.-Y. Ji, W.-P. Hu, L. Jiang, Y.-L. Song, D.-B. Zhu, *J. Mater. Chem*. **2007**, *17*, 90-94. b) A. Miniewicz, K. Palewska, L. Sznitho, J. Lipinski, *J. Phys. Chem. A* **2011**, *115*, 10689-10697.

[30] X. Y. He, A. C. Benniston, H. Saarenpaa, H. Lemmetyinen, N. V. Tkachenko, U. Baisch, *Chem. Sci.* **2015**, *6*, 3525-3532.

[31] M. de Jong, L. Seijo, A. Meijerink, F. T. Rabouw, *Phys. Chem. Chem. Phys*. **2015**, *17*, 16959-16969.

[32] S. Baderschneider, U. Scherf, J. Köhler, R. Hildner, *J. Phys. Chem. A* **2016**, *120*, 233-240.

[33] S. A. Vinogradov, M. A. Fernandez-Serra, B. W. Duggan, D. F. Wilson, *Rev. Sci. Instruments* **2001**, *72*, 3396-3406.

[34] S. F. Wuister, C. de Melo, A. Meijerink, *J. Phys. Chem. B* **2004**, *108*, 17393-17397.

[35] J. Tang, R. A. Marcus, *J. Chem. Phys*. **2005**, *123*, 204511.

[36] A. Harriman, M. A. H. Alamiry, J. P. Hagon, D. Hablot, R. Ziessel, *Angew. Chem., Int. Ed*. **2013**, *52*, 6611-6615.

[37] R. G. Allen, E. Johnson, V. Nagarajan, W. W. Parson, C. J. Law, R. G. Cogdell, *J. Phys. Chem. B* **1997**, *101*, 4667-4680.

[38] T. Förster, *Ann. Phys*. **1948**, *2*, 55-75.

[39] a) S. Saini, H. Singh, B. Bagchi, *J. Chem. Sci*. **2006**, *118*, 23-35: b) R. Ziessel, M. A. H. Alamiry, K. J. Elliott, A. Harriman, *Angew. Chem., Int.*

Ed. **2009**, *121*, 2810-2814: c) B. P. Krueger, G. D. Scholes, G. R. Fleming, *J. Phys. Chem. B* **1998**, *102*, 5378-5386.

[40] G. J. Hedley, A. Ruseckas, A. C. Benniston, A. Harriman, I. D. W. Samuel, *J. Phys. Chem. A* **2015**, *119*, 12665-12671.

[41] M. Spitler, M. Calvin, *J. Chem. Phys*. **1977**, *67*, 5193-5200.

[42] K. Kemnitz, N. Tamai, I. Yamazaki, N. Nakashima, K. Yoshihara, *J. Phys. Chem*. **1986**, *90*, 5094-5101.

[43] T. Fujii, H. Nishikiori, T. Tamura, *Chem. Phys. Lett*. **1995**, *233*, 424-429.

[44] T. A. Laurence, B. A. Chromy, *Nature Methods* **2010**, *7*, 338-339.

[45] J. W. Nichols, R. E. Pagano, *Biochem*. **1982**, *21*, 1720-1726.

[46] A. A. Istratov, O. F. Vyvenko, *Rev. Sci. Instr*. **1999**, *70*, 1233-1257.

[47] A. Siemiarczuk, B. D. Wagner, W. R. Ware, *J. Phys. Chem*. **1990**, *94*, 1661-1666.

[48] M. Vincent, J. Galley, A. P. Demchenko, *J. Phys. Chem*. **1995**, *99*, 14931-14941.

[49] F. Lopez Arbeloa, P. Ruiz Ojeda, I. Lopez Arbeloa, *J. Lumin*. **1989**, *44*, 105-112.

[50] D. Magde, J. H. Brannon, T. L. Cremers, J. Olmsted, *J. Phys. Chem*. **1979**, *83*, 696-699.

[51] G. Calzaferri, S. Huber, H. Maas, G. Minkowski, *Angew. Chem., Int. Ed*. **2003**, *42*, 3732-3758.

[52] a) J. Singh, E. R. Bittner, D. Beljonne, G. D. Scholes, *J. Chem. Phys*. **2009**, *131*, 194905: b) V. Stehr, B. Engels, C. Deibel, R. F. Fink, *J. Chem. Phys*. **2014**, *140*, 024503.

[53] a) C. Minkowski, R. Pansu, M. Takano, G. Calzaferri, *Adv. Funct. Mater*. **2006**, *16*, 273-285: b) H. Sigal, D. Markovitsi, L. K. Gallos, P. Argyrakis, *J. Phys. Chem*. **1996**, *100*, 10999-11004.

[54] W. H. Thompson, *J. Chem. Phys*. **2002**, *117*, 6618-6628.

[55] A. Adronov, S. L. Gilat, J. M. J. Frechet, K. Ohta, F. V. R. Neuwahl, G. R. Fleming, *J. Am. Chem. Soc*. **2000**, *122*, 1175-1186.

[56] a) Y. Nakamura, N. Aratani, A. Osuka, *Chem. Soc. Rev*. **2007**, *36*, 831-845: b) J. Z. Li, A. Ambroise, S. I. Yang, J. R. Diers, J. Seth, C. R. Wack, D. F. Bocian, D. Holten, J. S. Lindsey, *J. Am. Chem. Soc*. **1999**, *121*, 8927-8940: c) F. Giacalone, J. L. Segura, N. Martin, J. Ramey, D. M. Guldi, *Chem. Eur. J.* **2005**, *11*, 4819-4834.

[57] a) A. Harriman, R. Ziessel, *Chem. Commun*. **2011**, *47*, 611-631: b) A. Harriman, L. J. Mallon, K. J. Elliott, A. Haefele, G. Ulrich, R. Ziessel, *J. Am. Chem. Soc*. **2009**, *131*, 13375-13386: c) R. W. Wagner, T. E. Johnson, J. S. Lindsey, *J. Am. Chem. Soc*. **1996**, *118*, 11166-11180.

[58] a) R. van Grondelle, V. I. Novoderezhkin, *Phys. Chem. Chem. Phys*. **2006**, *8*, 793-807: b) M. Chachisvilis, O. Kuhn, T. Pullerits, V. Sundstrom, *J. Phys. Chem. B* **1997**, *101*, 7275-7283: c) V. Tiwani, W. K. Peters, D. M. Jonas, *Proc. Natl. Acad. Sci*. **2013**, *110*, 1203-1208.

[59] a) A. Ishizaki, G. R. Fleming, *Proc. Natl. Acad. Sci*. **2009**, *106*, 17255-17260: b) J. Adolphs, T. Renger, *Biophys. J*. **2006**, *91*, 2778-2797: c) D. Beljonne, C. Curutchet, G. D. Scholes, R. J. Silbey, *J. Phys. Chem. B* **2009**, *113*, 6583-6599.

[60] A. R. Clapp, I. L. Medintz, H. Mattoussi, *ChemPhysChem* **2006**, *7*, 47-57.

[61] H. Sumi, *J. Phys. Chem. B* **1999**, *103*, 252-260.

[62] A. Datta, S. K. Pati, *J. Chem. Phys*. **2003**, *118*, 8420-8427.

[63] C.-P. Hsu, Z.-Q. You, H.-C. H. Chen, *J. Phys. Chem. C* **2008**, *112*, 1204-1212.

[64] C. H. Bennett, D. P. Di Vencenzo, *Nature* **2000**, *404*, 247-255.

[65] P. Blood, *Quantum Confined Laser Devices*, Oxford Master Series in Atomic, Optical and Laser Physics, Oxford University Press, Oxford, 2015.

[66] J. Olmsted III, *J. Phys. Chem*. **1979**, *83*, 2581-2584.

[67] D. V. O'Connor, D. Phillips, *Time-correlated, Single Photon Counting*, Academic Press, London, 1984.

[68] R. C. Clark, J. S. Reid, *Acta Cryst. A* **1995**, *A51*, 887-897.

[69] O. V. Dolomanov, L. J. Bourhis, R. J. Gildea, J. A. K. Howard, H. Puschmann, *J. Appl. Cryst*. **2009**, *42*, 339-341.

Entry for the Table of Contents

FULL PAPER

An artificial light-harvesting membrane has been fabricated by dispersing emissive crystals doped with Rhodamine B. Rapid exciton migration occurs within the bulk of the crystal, followed by trapping at the surface and subsequent energy transfer to the fluorescent dopant.

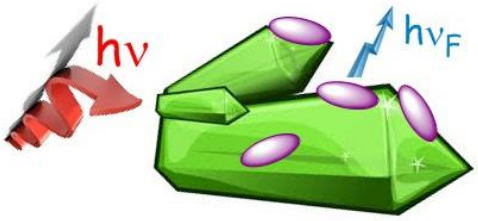

Roza Al-Aqar, Alparslan Atahan, Andrew C. Benniston, Thomas Perks, Paul G. Waddell and Anthony Harriman

Page No. – Page No.

Exciton Migration and Surface Trapping for a Photonic Crystal Displaying Charge-Recombination Fluorescence